BIOCHEMISTRY

 Volume 45, Number 10 March 14, 2006

Accelerated Publications

Microsecond Time Scale Rotation Measurements of Single F_1-ATPase Molecules†

David Spetzler,‡ Justin York,‡ Douglas Daniel, Raimund Fromme, David Lowry, and Wayne Frasch*

Faculty of Biomedicine and Biotechnology, School of Life Sciences, Arizona State University, P.O. Box 874501, Tempe, Arizona 85287-4501

Received November 18, 2005; Revised Manuscript Received December 20, 2005

ABSTRACT: A novel method for detecting F_1-ATPase rotation in a manner sufficiently sensitive to achieve acquisition rates with a time resolution of 2.5 μs (equivalent to 400 000 fps) is reported. This is sufficient for resolving the rate at which the γ-subunit travels from one dwell state to another (transition time). Rotation is detected via a gold nanorod attached to the rotating γ-subunit of an immobilized F_1-ATPase. Variations in scattered light intensity allow precise measurement of changes in the angular position of the rod below the diffraction limit of light. Using this approach, the transition time of *Escherichia coli* F_1-ATPase γ-subunit rotation was determined to be 7.62 ± 0.15 (standard deviation) rad/ms. The average rate-limiting dwell time between rotation events observed at the saturating substrate concentration was 8.03 ms, comparable to the observed Mg^{2+}-ATPase k_{cat} of 130 s^{-1} (7.7 ms). Histograms of scattered light intensity from ATP-dependent nanorod rotation as a function of polarization angle allowed the determination of the nanorod orientation with respect to the axis of rotation and plane of polarization. This information allowed the drag coefficient to be determined, which implied that the instantaneous torque generated by F_1 was 63.3 ± 2.9 pN nm. The high temporal resolution of rotation allowed the measurement of the instantaneous torque of F_1, resulting in direct implications for its rotational mechanism.

The F_1F_o-ATP synthase couples the energy provided by a transmembrane proton gradient to the production of ATP from ADP and phosphate. The intrinsic membrane complex of ab_2c_{10-14} subunits known as F_o[1] functions as a proton channel, and the F_1 peripheral membrane complex of $\alpha_3\beta_3\gamma\delta\epsilon$ subunits contains one site for ATP synthesis and/or hydrolysis per $\alpha\beta$ heterodimer. When F_1 is purified from F_o and the membrane, it retains the ability to hydrolyze ATP (*1*−*3*). There are three catalytic sites which are coupled such that the binding of the substrate to one site induces conformational changes that result in product release at an adjacent site. The three heterodimers form a ring around the γ-subunit that rotates in response to ATP hydrolysis activity (*4*, *5*).

Visualization of γ-subunit rotation of single F_1 molecules fixed to a coverslip can be observed by microscopy (*6*, *7*). Rotation appears as discrete 120° steps for each Mg^{2+}-ATP consumed at saturating Mg^{2+}-ATP concentrations. When the substrate is limiting, each 120° step is resolved into 80° and 40° substeps that correspond to ATP binding and the rate-limiting step, respectively (*6*, *8*). Binding of Mg^{2+}-ATP to the empty catalytic site was found to initiate a 80° rotation of the γ-subunit in F_1 from the thermophilic bacteria *PS3* (*9*). After a 2 ms pause thought to involve product release, a 40° rotation of the γ-subunit completes the cycle for a

† This work was supported by National Institutes of Health Grant GM50202 to W.D.F.

* To whom correspondence should be addressed. E-mail: frasch@asu.edu. Telephone: (480) 965-8663. Fax: (480) 965-6899.

‡ These authors contributed equally to this work.

[1] Abbreviations: F_1, extrinsic membrane-associated protein complex of F_1F_o-ATP synthase; F_o, intrinsic membrane protein complex of F_1F_o-ATP synthase; fps, frames per second.

10.1021/bi052363n CCC: $33.50
Published on Web 02/17/2006

total of 120°. The kinetics of the 2 ms pause are consistent with the presence of sequential 1 ms steps which suggest the existence of a rate-limiting intermediate state that follows the transition state (*10*, *11*). Recent experiments may indicate that the completion of a catalytic cycle at any one site involves the rotation of the γ-subunit by 240° (*6*, *12*−*15*).

The rotation of F_1-ATPase has been observed using large actin filaments, where the rate is dependent upon the viscous drag of the reporter group, not the intrinsic mechanism of the enzyme (*16*, *17*). It has been reported that the viscous drag of 40 nm diameter gold nanospheres does not limit the rate of rotation (*6*). These probes have been used to measure the pause or dwell time between rotation events via determination of the centroid of light scattered from the probe. However, under these conditions, attempts to measure the rate of rotation between dwells with recording speeds as high as 8000 fps were insufficient for measuring the velocity of the γ-subunit as it rotates from one dwell to the next. We now report a method for recording F_1-ATPase γ-subunit rotation with a time resolution of 2.5 μs (equivalent to 400 000 fps), which resolves the velocity of the γ-subunit as it rotates between dwells.

EXPERIMENTAL PROCEDURES

Escherichia coli F_1-ATPase was purified from strain XL10 (*18*). This strain was mutated to contain a His_6 on the N-terminus of the α-subunit and γS193C for biotinylation. Biotinylation was performed by adding an equimolar amount of biotin-maleimide (Pierce) to F_1, followed by shaking at room temperature for 1 h. Unreacted biotin-maleimide was removed after the solution was run through a protein desalting column (Pierce). Reaction specificity to the γ-subunit was verified by SDS−PAGE with a fluorescent maleimide. The activity of the enzyme was confirmed using the pyruvate kinase coupled assay (*18*−*20*).

Gold nanorods were prepared by the reduction of $HAuCl_4$ to form 4 nm seeds (*21*). The seeds were grown into gold nanorods in the presence of the surfactant CTAB and additional $HAuCl_4$. The length and width of the gold rods were determined to be 75.08 ± 4.1 and 34.7 ± 2.2 nm, respectively ($N = 30$), using transmission electron microscopy. Avidination of gold rods began with an exchange of the gold rod buffer (100 mM CTAB) with 1 mM CTAB. Neutravidin was added directly to the nanorod/CTAB solution to a final concentration of 40 μg/mL. The mixture was shaken at room temperature for 1 h and could be stored at room temperature for up to 1 week. Successful avidination was verified by observing a 4−10 nm red shift in the absorbance spectrum of the gold nanorods (Figure 1). This red shift was attributed to a change in the dielectric environment of the gold nanorod surface (*22*). For use in the rotation assay, avidinated gold nanorods were further diluted 1:10 in F_1 buffer [50 mM Tris-HCl and 10 mM KCl (pH 8.0)] containing 0.1% modified BSA.

In a typical experiment, a Ni−NTA resin-coated glass slide was spotted with 5 μL of 85 μg/mL F_1 such that the F_1 molecules became immobilized to the Ni−NTA resin via the three His_6 tags. After a 5 min incubation, the slide was washed for 30 s with F_1 buffer. After excess liquid was wicked from the surface, the spot containing immobilized F_1 was exposed to 5 μL of avidinated gold nanorods for 5 min. A final 30 s wash with F_1 buffer removed unbound and nonspecifically bound gold nanorods. Excess liquid was wicked away, and 5 μL of 2 mM $MgCl_2$ and 1 mM ATP in F_1 buffer was added.

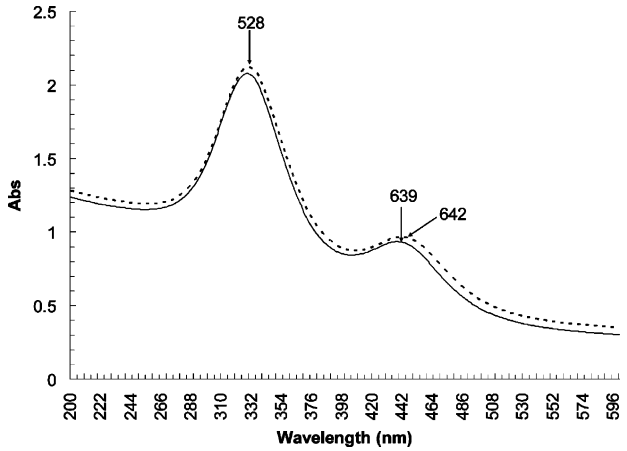

FIGURE 1: Absorption spectra of gold nanorods before and after coating with avidin. Prior to avidination (bottom trace), gold spheres and nanorods absorb 529 and 639 nm light, respectively. Incubation of the gold rods with avidin (top trace) results in a red shift of the nanorod absorption to 642 nm.

A Leica DMIRE II inverted dark-field microscope was used to obtain quantitative data for gold nanorod rotation driven by F_1. A Sutter LB-17 xenon light with a custom Chroma cold mirror was coupled with a Series 2000 Lumatec light guide to deliver 400−925 nm collimated light to the dark-field condenser. The light not scattered by a gold nanorod was stopped by an iris in the 63× variable-aperture objective. Scattered light from single molecules was focused onto a 100 μm pinhole mounted on an xyz translation stage (Thorlabs) in the image plane at the microscope side port. The pinhole acted as a spatial filter, blocking all light except that originating from the molecule under study. The scattered light then passed through a polarization filter mounted in a rotational stage (Standa, 8SMC1-USB) and was refocused onto a single photon counting avalanche photodiode (Perkin-Elmer SPCM-AQR-15). The detector has a dark count of ∼50 photons/s with a temporal resolution of 50 ns, equivalent to 20 million fps. Single rotating rods were positioned confocal to the pinhole using a motorized stage from Prior Scientific (0.002 μm/micro-step resolution) and a digital camera (Optronics, MagnaFire SP). The refresh rate of the camera was sufficiently fast to detect the strobe effect due to rotation, which allowed identification of the rotating gold nanorods and their corresponding alignment to the photon counter. Output from the detector was fed directly into a National Instruments DAQ PCI-6602 counter/timer board. Custom software was written in LabView 7.1 to control data acquisition, storage, and analysis of dwell times. Additional custom software was written in Matlab 6.5 to compute the rate of rotation (transition time).

RESULTS

The optical properties of gold nanorods were exploited in taking sensitive measurements of rotational position. When viewed using dark-field microscopy, an 75 nm × 35 nm nanorod resonantly scatters red and green light from the long and short axis of the rod, respectively (*23*). Incident light

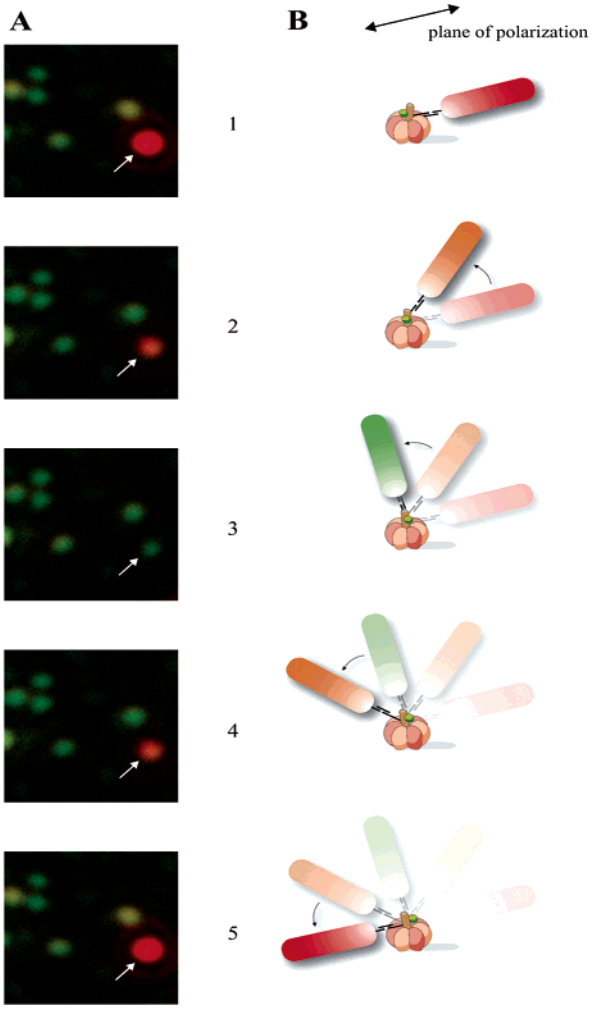

FIGURE 2: Light scattering properties of gold nanorods viewed through a polarizing filter. (A) Consecutive dark-field micrographs of a stationary rod observed when (1) the plane of polarization is parallel to the long axis of the rod and (2−5) the filter was rotated in 45° increments. (B) Schematic of a gold nanorod attached to the F_1 γ-subunit as it would rotate vs A.

illuminated the sample at an oblique angle so that only light scattered from the nanorods entered the objective. When scattered light from a nanorod was viewed through a polarizing filter, its intensity changed as a function of the relative angle between its longitudinal and translational axes and the polarizing filter (Figure 2A). Light is scattered most efficiently along the rod axes such that the intensity of scattered red light is maximal and minimal when the long and short axes of the rod are parallel and orthogonal to the plane of polarization, respectively. The converse is true for the intensity of scattered green light. Therefore, the intensities of light scattered from a gold nanorod immobilized to a single F_1 γ-subunit change as a function of the polarization angle (Figure 2B). The resulting intensity profiles of red and green light follow out-of-phase sine curves.

To measure Mg^{2+}-ATP-dependent γ-subunit rotation, the intensity of red light scattered from single nanorods was acquired as a function of time. As a control, the scattered light intensity at a given rate of data acquisition was established when the rod was not rotating (Figure 3A). The signal generated by the nanorod in the presence of 1 mM $MgCl_2$ and 2 mM ATP, acquired at the same collection rate

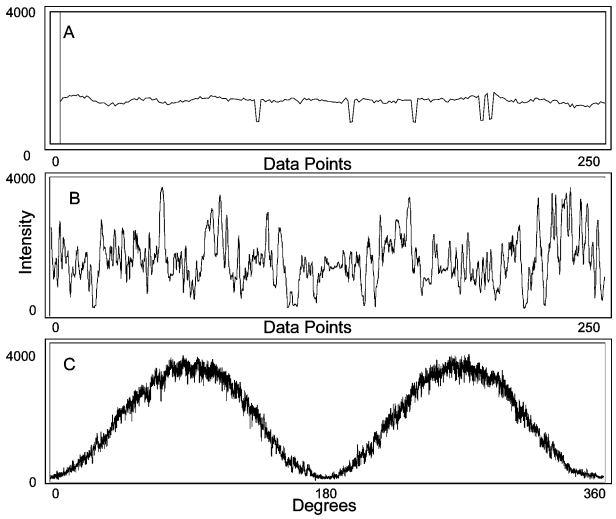

FIGURE 3: Confirmation of F_1-dependent rotation of a gold nanorod using a single photon counter. Data sets of the same gold rod were collected after assembly with F_1 at an acquisition rate of 1 kHz. Scattered red light intensity profiles of the gold nanorod were measured (A) while it was not rotating, (B) during ATP-dependent F_1 rotation, and (C) while the rod was stationary but the polarizer was rotated 360° to establish maximum and minimum intensity values of scattered red light.

and scale, is shown in Figure 3B. To establish the maximum and minimum intensities of scattered light at that data acquisition rate, the polarizing filter was rotated when the nanorod was not rotating (Figure 3C). The observed depth of oscillation in the presence of substrate was consistent with the intensity range predicted by Figure 3C, indicating that the variation in signal was due to Mg^{2+}-ATP-dependent γ-subunit rotation. The average rate-limiting dwell time from 22 molecules was determined to be 8.3 ms. The k_{cat} of Mg^{2+}-ATP hydrolysis for these F_1 preparations was 130 s^{-1} (7.7 ms) at 1 mM Mg^{2+}-ATP, which is consistent with the 8.3 ms rate-limiting dwell observed between rotational events.

The minimum and maximum intensity values occur when the rod is perpendicular and parallel to the plane of polarization, respectively. Therefore, transitions between these extremes correspond to rotation of the gold nanorod by 90°. Figure 4A shows γ-subunit rotation data collected at 400 kHz when the polarizing lens was aligned with one of the dwell states parallel to the plane of polarization (Figure 4B). Consequently, when aligned as in Figure 4C, a 120° rotational event from dwell position I to II would cause the rod to begin at an intermediate intensity value, pass through a minimum, and end near a maximum. The converse is true for rotation events from dwell position II to III. Rotation data from dwell position III to I do not span the entire range of light intensity and thus did not meet the selection criteria for further analysis.

The stochastic nature of each rotational event makes it difficult to determine the rod position at the start and end of any single rotation event. Since the most sensitive measure of the 120° rotation is the 90° subset that caused a change between minimum and maximum intensity values, these changes were used to measure rotation rate. The effects of intensity range and linearity on the calculation of transition time were determined. Figure 5 shows the average calculated transition time as a function of R^2 values which span five

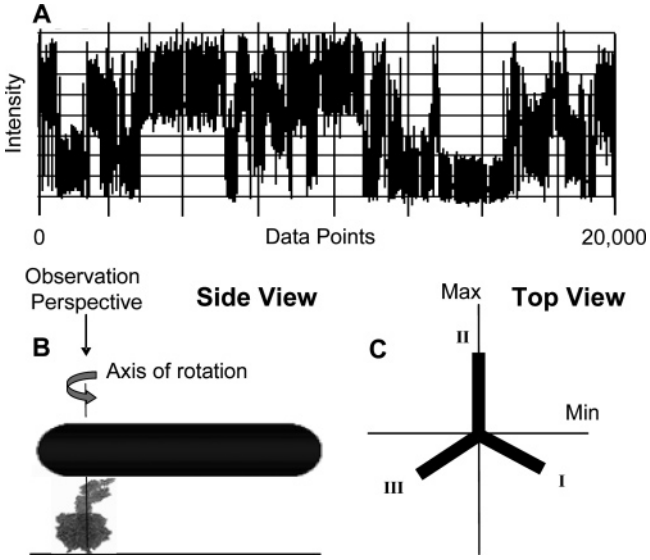

FIGURE 4: Measurements of F_1-ATPase γ-subunit rotation. (A) F_1-ATPase rotation-dependent changes in scattered red light intensity collected at 400 kHz. (B) Schematic of the rod orientation between F_1 and the plane of polarization. Approximate position of dwell states I−III relative to the maximum and minimum intensity values of scattered red light.

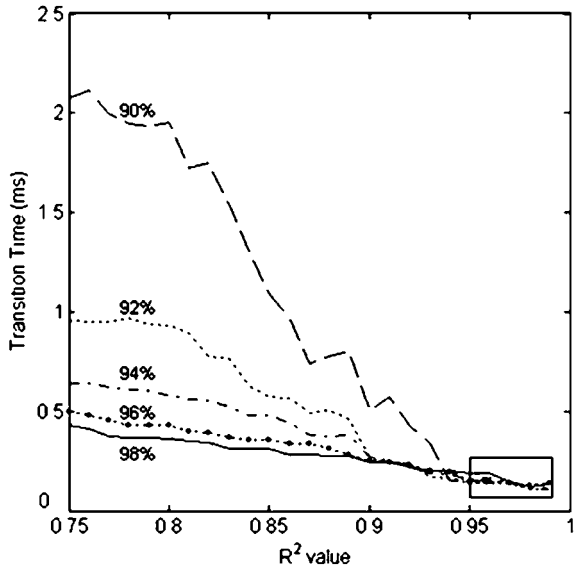

FIGURE 5: Effects of data selection criteria on the calculated transition time. Transition times were calculated as a function of R^2 values from light intensity changes between percentile ranges from 99th to 1st (98%), 98th to 2nd (96%), 97th to 3rd (94%), 96th to 4th (92%), and 95th to 5th (90%). The difference in the calculated transition time is not sensitive to the R^2 values greater than 0.95 for each percentile range as shown in the boxed region.

different intensity ranges. When transitions that spanned 90% of the total possible range were considered, there was substantial variation for R^2 values of <0.95. As larger intensity ranges were considered, the calculated transition time was more consistent as the R^2 value decreased. Calculated transition times converged to similar values for data that spanned at least 90% of the total intensity range and had R^2 values greater than 0.95.

An example transition from a data set collected at 400 kHz is shown in Figure 6A. This transition, which had an R^2 value of 0.987 from a linear least-squares regression, did not contain any apparent variation in rate over the 90° of rotation that was assessed. The variation of transitions that satisfy the selection criteria is shown in Figure 6B. Most events show a constant slope during rotation. However, there is evidence of a short pause in some of the transitions. Although each 120° step is composed of 80° and 40° substeps, the stochastic nature of a single rotational event causes variability in the proportion of 80° and 40° substeps that are included in any 90° data acquisition. Therefore, attempts to distinguish differences in the transition time of these substeps were not made.

Figure 7 depicts the average time required for the γ-subunit to rotate 90° as a function of the data acquisition rate to show the minimum acquisition rate required to resolve the sweep time. These measurements were obtained at resolutions between 100 and 2.5 μs (equivalent to acquisition rates of 10000−400000 fps). The transition time calculated from data acquired at rates faster than 50 kHz showed no significant deviation. The average transition time from these data for 22 F_1 molecules containing more than 72 000 rotational events was determined to be 7.62 ± 0.15 (standard deviation) rad/ms.

Each catalytic event can be examined as both a dwell associated with the rate-limiting step and a rotational transition related to the power stroke of an engine. Torque generated by F_1 is calculated using the laminar flow Stokes equation

$$T = \omega\xi \tag{1}$$

where ω is the angular velocity and ξ is the drag coefficient. However, torque changes with the drag coefficient depending upon how the rod binds to the γ-subunit according to the following equation:

$$\xi = 16\pi\eta\alpha^3 + 12\pi\eta\alpha{x_1}^2 + 12\pi\eta\alpha{x_2}^2 \tag{2}$$

where α is the nanorod radius, x_1 and x_2 correspond to the length of the nanorod in terms of the attachment point, and η is the viscosity of the medium (1×10^{-3} N s m^{-2} at 25 °C). However, to use this equation, knowledge of the nanorod orientation relative to the axis of rotation is required. Since this information is not generally available, it has been assumed that, on average, attachment of the γ-subunit to the

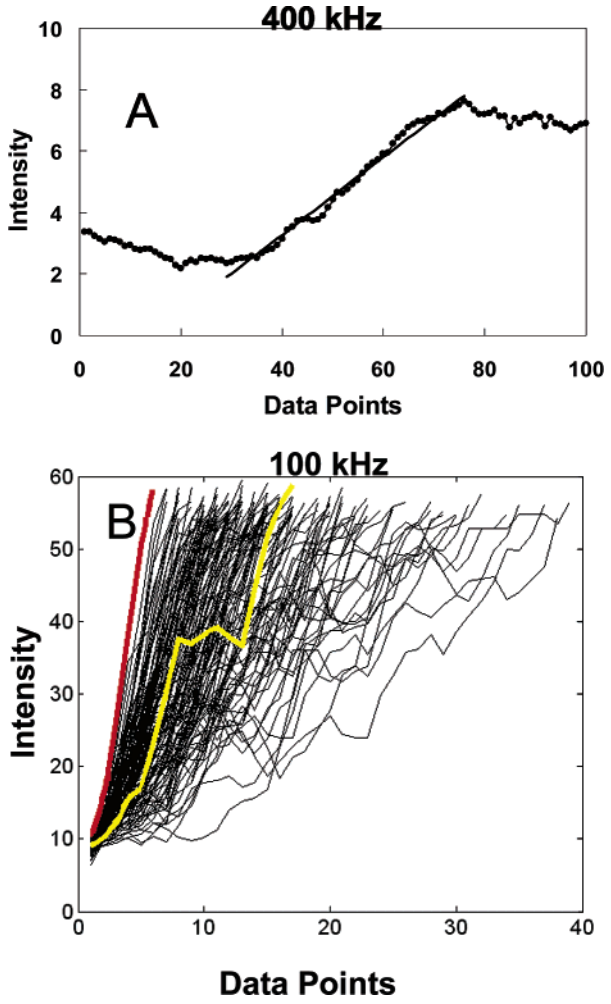

FIGURE 6: Subset of rotational events. (A) A single transition from the data set in Figure 4A showing data points and the associated trend line ($R^2 = 0.987$). (B) Superposition of transitions acquired at 100 kHz. The transition depicted in red is representative of the fastest and most common type of transition observed. The transition depicted in yellow represents a subpopulation of events that contain an intermediate pause.

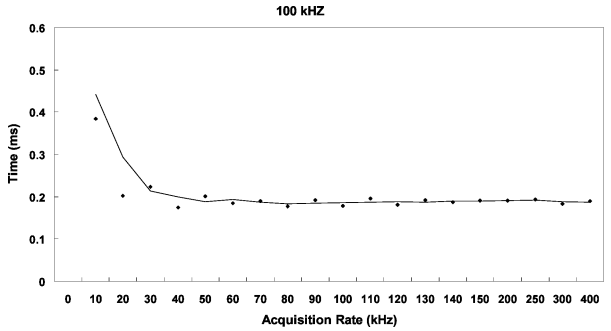

FIGURE 7: Average transition time calculated from data collected from five F_1 molecules at acquisition rates between 10 and 400 kHz.

nanoparticle occurs near the middle of its longitudinal axis so that ξ can be modeled by

$$\xi = 8\pi\eta\alpha^3 + 6\pi\eta\alpha x^2 \quad (3)$$

On the basis of eq 3, a constant velocity of 7.62 rad/ms implies that the average torque generated by the γ-subunit is ~47.4 ± 4.2 pN nm, similar to values reported elsewhere (*1*, *24*).

Information concerning the orientation of a gold nanorod relative to the axis of rotation and the plane of polarization was obtained by examining the relationship between time-averaged locations of the three dwells and the angle of the polarizing filter. When the axis of rotation is orthonormal to the plane of polarization, three peaks in the histograms of the intensity values should be observed that correspond to each dwell. As the polarizer is rotated, the contribution of each dwell state should follow three sine curves offset by 60° (Figure 8A). The following equation models the behavior of the F_1 molecule when it is aligned as in Figure 8A

$$F_x = \frac{\alpha\left[\sin(X_1) + \sin\left(X_2 + \frac{2\pi}{3}\right) + \sin\left(X_3 + \frac{4\pi}{3}\right) + 3\right]}{3} \quad (4)$$

where α is a scaling term dependent upon the data acquisition rate and each X represents a normally distributed population of values for relative positions of the dwell states to the polarization filter.

Panels B and D of Figure 8 show histograms of dwell states during ATP-dependent rotation when the polarized lens was oriented such that a dwell was aligned with maximum and minimum intensity values, respectively. In these cases, two peaks overlap and were maximally spaced from the other as predicted by alignment of states B and D in Figure 8A. When the polarized lens was moved out of alignment with a dwell state, light intensity values of the three dwell states diverged (Figure 8C), as predicted by alignment state C in Figure 8A. Therefore, the orientation of the gold rod to the axis of rotation and the plane of polarization can be determined by observing the changes in the relationship between intensity peaks as a function of the polarization angle. Of the 22 molecules examined, 19 exhibited this behavior.

The three remaining molecules did not follow the pattern predicted by the model described by eq 4. Figure 9A shows consecutive histograms of intensity values as a function of the polarization angle during ATP-dependent rotation of one such molecule. When viewed collectively, only two dwell states offset by 90° were observed. This observation strongly suggests a molecule orientation where the axis of rotation of the γ-subunit was at a 45° angle with respect to the plane of polarization, and the end of the longitudinal axis of the gold nanorod was bound at a 45° angle with respect to the γ-subunit (Figure 9C). This configuration likely resulted from variation in the glass surface and the location of attachment of avidin to the gold nanorod. The motion of the gold rod was limited to a cone oriented such that the tip of the cone was at the axis of rotation and the body was contained within a single octant. In this case, the projection of the rod onto the plane of polarization would result in one state contributing a constant minimum intensity value while the other two states appear to be 90° from one another. Consequently, an intensity change from the minimum to the maximum values should correspond to rotation of the γ-subunit by 120° rather than 90°.

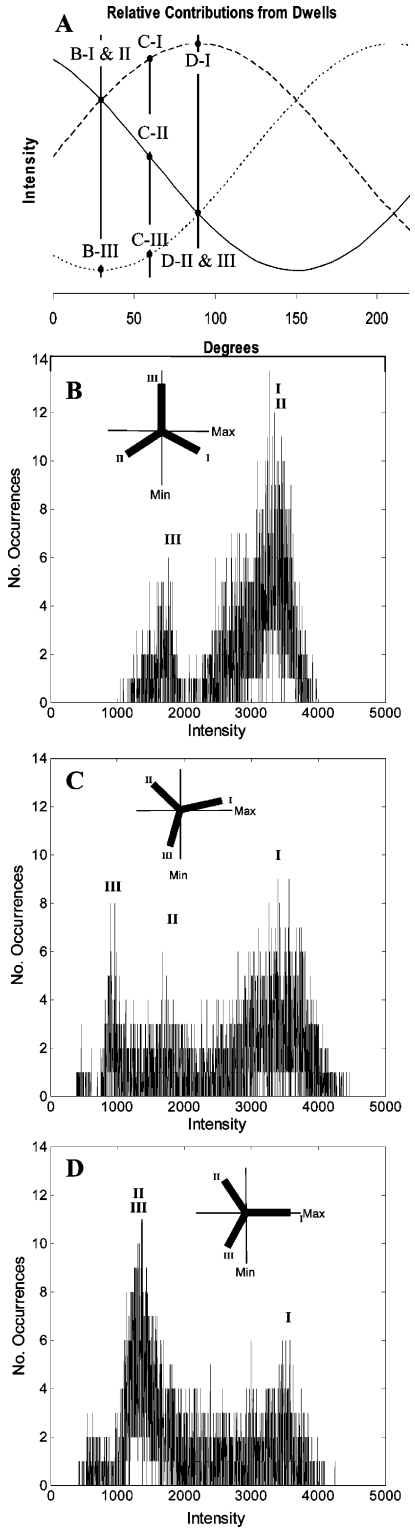

FIGURE 8: Contributions of dwell states to the intensity profile as a function of polarizing filter alignment acquired at 1 kHz. (A) Simulation of relative contributions from each dwell when the axis of rotation is orthonormal to the plane of polarization. As the polarizer is rotated, the contribution of each dwell state is modeled by three sine curves offset by 60°. Vertical lines B−D correspond to relative dwell locations depicted in the insets of panels B−D. Intersections between the sine curves and the vertical lines correspond to peaks in the intensity profiles. (B−D) Histograms of intensity values from rotation data acquired at 1 kHz when the orientations between the plane of polarization and dwell states occur as depicted in the respective insets. Positions I−III represent consecutive dwell states which contribute to intensity peaks as labeled.

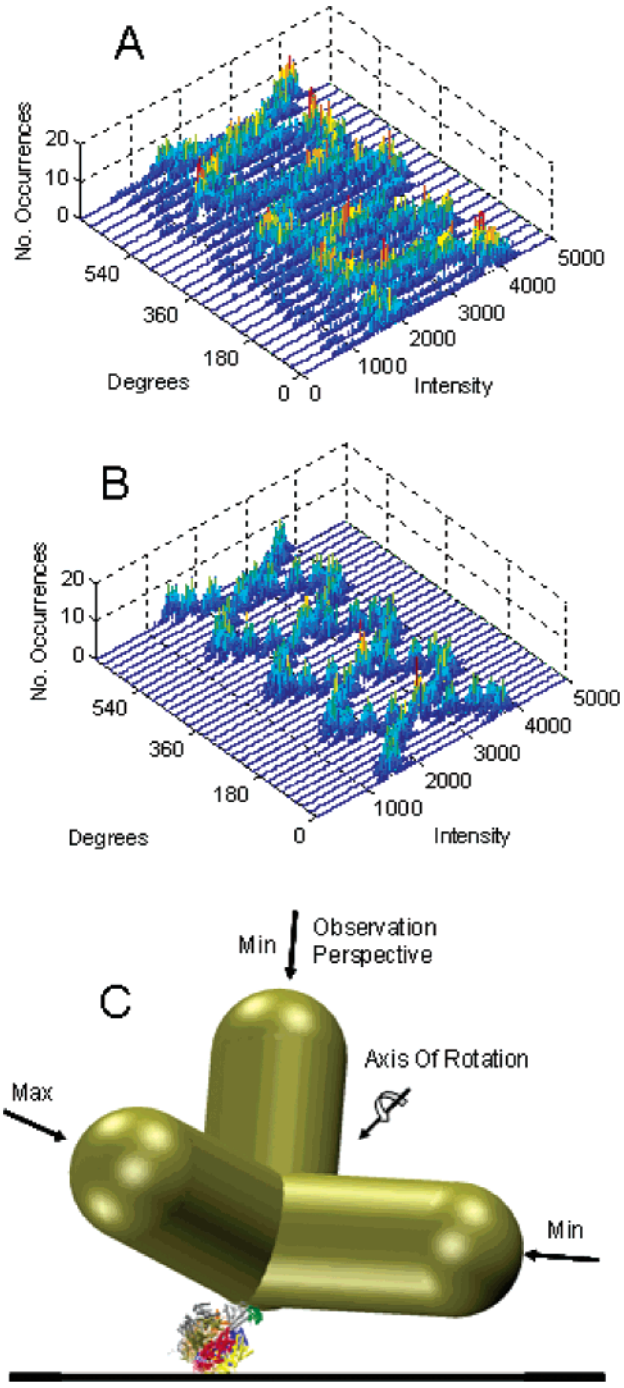

FIGURE 9: Consecutive histograms of intensity values as a function of the polarization angle during ATP-dependent rotation. Histogram series of experimental results from a single molecule (A) and simulated results (B) of intensity values as a function of the relative angle between the plane of polarization and the dwell states. (C) Three-dimensional model of rod orientation, where the projection of the dwell states into the two-dimensional viewing plane results in two distinguishable states that appear 90° apart.

A simulation of the changes in the histograms as a function of the angle of polarization (Figure 9B) was generated using the following function:

$$F_x = \frac{\alpha[\sin(X_1) + \sin(X_2 + \pi) + \phi(X_3) + 3]}{3} \qquad (5)$$

This equation models the behavior of the F_1 molecule when it is aligned as in Figure 9C, where α is a scaling term

dependent upon the data acquisition rate. Each X_n represents a normally distributed population of values for relative positions of the polarization filter. The function $\phi(X_3)$ is a term for the contribution of the dwell state that is aligned with the observation perspective. The observed behavior of the molecules was consistent with the trends predicted by the model. In addition, the instantaneous velocity of these three molecules was consistent with values determined for the other molecules traveling 90° when these molecules were assumed to rotate 120°. Both results support the proposed orientation of the axis of rotation and nanorod attachment. On the basis of this orientation of the gold nanorod, eq 2 was used to calculate the instantaneous torque of 63.3 ± 2.9 pN nm for these F_1 molecules.

DISCUSSION

Rotation of the F_1 γ-subunit was first measured using an actin filament probe where the rate of rotation was limited by the viscous drag of the filament (*16*, *17*). Minimal differences observed between rotation rates using gold beads 40 and 60 nm in diameter suggest that the viscous drag does not limit the rate of rotation (*25*, *26*). Since the 75 nm × 35 nm rods have an effective drag between that observed for the 40 and 60 nm beads, it is likely that the intrinsic mechanism of the enzyme limits the rate of rotation.

The results presented here show that the instantaneous velocity of γ-subunit rotation occurs at a constant rate of 7.62 ± 0.15 (standard deviation) rad/ms. This measurement was made using a novel technology capable of achieving a temporal resolution of 2.5 μs (400 kHz). The measurement was confirmed by comparing transition times observed at increasing acquisition rates, until the transition time was independent of the temporal resolution. This occurred at an acquisition rate of at least 50 kHz, corresponding to a resolution of 20 μs.

Observed dwell times at saturating substrate concentrations were consistent with bulk measurements of *E. coli* F_1 Mg^{2+}-ATPase activity. The average dwell time was 8.3 ms, which was substantially longer than that measured in F_1 from the thermophilic bacterium *PS3* (*6*). Dwells were best resolved at an acquisition rate of 1 kHz such that each dwell measurement was the sum of the time spent pausing and rotating. Consequently, the actual dwell time for *E. coli* F_1 is ~8.03 ms since it takes approximately 0.27 ms for the γ-subunit to rotate 120° during a single catalytic event.

On the basis of the results presented here, the average torque generated during rotation was ~47.4 ± 4.2 pN nm, comparable to that previously reported for F_1 from *PS3* (*1*, *24*, *27*). The maximum observed torque was determined to be 63.3 ± 2.9 pN nm for those molecules oriented as in Figure 9. A factor that could affect the torque is increased viscous drag due to the interfacial properties of ordered water near the surface of the slide. However, these effects become minimal more than 2−3 nm from the surface (*28*, *29*). The biotinylation site of the γ-subunit is ~12 nm from the surface, and therefore, these interfacial effects on the drag coefficient should be negligible. The calculated work done by F_1 during a single transition was, on average, 99.3 ± 8.8 pN nm. Since the gold rod is unlikely to limit the rate of rotation, the work done will be the minimum required to move it. The potential work that can be done during a single transition may be greater than the actual work needed to move the rod, implying that existing measurements are likely to underestimate the possible torque. Thus, any measurement that results in a larger torque value is likely to reflect the potential torque of the motor. The maximum amount of work observed during a 120° transition was 132.5 ± 6.0 pN nm. This is significantly larger than the free energy of ATP hydrolysis (90 pN nm) under physiological conditions (*8*). Therefore, the observed torque generated by the motor cannot be explained by the free energy of ATP hydrolysis alone. Another possible source of free energy might be derived from the differences in affinities for the substrate and product in the catalytic site under conditions of a favorable chemical gradient (*30*).

ACKNOWLEDGMENT

We thank Matthew Barber, Ana Bengston, Lars Chapsky, Matthew Green, and Liyan He for insightful conversations.

SUPPORTING INFORMATION AVAILABLE

Movie showing the strobe effect used to identify rotating gold nanorods. This material is available free of charge via the Internet at http://pubs.acs.org.

REFERENCES

1. Kinosita, K., Jr., Adachi, K., and Itoh, H. (2004) Rotation of F1-ATPase: How an ATP-driven molecular machine may work, *Annu. Rev. Biophys. Biomol. Struct. 33*, 245−68.
2. Senior, A. E., and Weber, J. (2004) Happy motoring with ATP synthase, *Nat. Struct. Mol. Biol. 11*, 110−2.
3. Walker, J. E., Saraste, M., and Gay, N. J. (1982) *Escherichia coli* F1-Atpase Interacts with a Membrane-Protein Component of a Proton Channel, *Nature 298*, 867−9.
4. Boyer, P. D. (1997) The ATP synthase: A splendid molecular machine, *Annu. Rev. Biochem. 66*, 717−49.
5. Junge, W., Lill, H., and Engelbrecht, S. (1997) ATP synthase: An electrochemical transducer with rotatory mechanics, *Trends Biochem. Sci. 22*, 420−3.
6. Noji, H., Yasuda, R., Yoshida, M., and Kinosita, K., Jr. (1997) Direct observation of the rotation of F1-ATPase, *Nature 386*, 299−302.
7. Kinosita, K., Jr. (1999) Real time imaging of rotating molecular machines, *FASEB J. 13* (Suppl. 2), S201−8.
8. Shimabukuro, K., Yasuda, R., Muneyuki, E., Hara, K. Y., Kinosita, K., Jr., and Yoshida, M. (2003) Catalysis and rotation of F1 motor: Cleavage of ATP at the catalytic site occurs in 1 ms before 40° substep rotation, *Proc. Natl. Acad. Sci. U.S.A. 100*, 14731−6.
9. Yoshida, M., Noji, H., and Muneyuki, E. (1997) [World smallest motor, ATP synthase], *Tanpakushitsu Kakusan Koso 42*, 1396−406.
10. Kinosita, K., Jr., Yasuda, R., Noji, H., and Adachi, K. (2000) A rotary molecular motor that can work at near 100% efficiency, *Philos. Trans. R. Soc. London, Ser. B Biol. Sci. 355*, 473−89.
11. Yoshida, M., Muneyuki, E., and Hisabori, T. (2001) ATP synthase: A marvellous rotary engine of the cell, *Nat. Rev. Mol. Cell Biol. 2*, 669−77.
12. Boyer, P. D., and Kohlbrenner, W. (1981) in *Energy Coupling in Photosynthesis* (Selman, S. S.-R., Ed.) pp 231−40, Elsevier, Amsterdam.
13. Duncan, T. M., Bulygin, V. V., Zhou, Y., Hutcheon, M. L., and Cross, R. L. (1995) Rotation of subunits during catalysis by *Escherichia coli* F1-ATPase, *Proc. Natl. Acad. Sci. U.S.A. 92*, 10964−8.
14. Sabbert, D., Engelbrecht, S., and Junge, W. (1996) Intersubunit rotation in active F-ATPase, *Nature 381*, 623−5.
15. Senior, A. E., Nadanaciva, S., and Weber, J. (2002) The molecular mechanism of ATP synthesis by F1F0-ATP synthase, *Biochim. Biophys. Acta 1553*, 188−211.
16. Panke, O., Cherepanov, D. A., Gumbiowski, K., Engelbrecht, S., and Junge, W. (2002) Viscoelastic dynamics of actin filaments

coupled to rotary F-ATPase: Angular torque profile of the enzyme, *Biophys. J. 83*, 582.
17. Panke, O., Cherepanov, D. A., Gumbiowski, K., Engelbrecht, S., and Junge, W. (2001) Viscoelastic dynamics of actin filaments coupled to rotary F-ATPase: Angular torque profile of the enzyme, *Biophys. J. 81*, 1220−33.
18. Greene, M. D., and Frasch, W. D. (2003) Interactions among γR268, γQ269, and the β subunit catch loop of *Escherichia coli* F1-ATPase are important for catalytic activity, *J. Biol. Chem. 278*, 51594−8.
19. Lowry, D. S., and Frasch, W. D. (2005) Interactions between βD372 and γ subunit N-terminus residues γK9 and γS12 are important to catalytic activity catalyzed by *Escherichia coli* F_1F_0-ATP synthase, *Biochemistry 44*, 7275−81.
20. Boltz, K. W., and Frasch, W. D. (2005) Interactions of γT273 and γE275 with the β subunit PSAV segment that links the γ subunit to the catalytic site Walker homology B aspartate are important to the function of *Escherichia coli* F_1F_0 ATP synthase, *Biochemistry 44*, 9497−506.
21. Jana, N. R., Gearheart, L., and Murphy, C. J. (2001) Wet Chemical Synthesis of high aspect ratio cylindrical gold nanorods, *J. Phys. Chem. B 105*, 4065−7.
22. Raschke, G., Kowarik, S., Franzl, T., Sonnichsen, C., Klar, T. A., Feldmann, J., Nichtl, A., and Kurzinger, K. (2003) Biomolecular recognition based on single gold nanoparticle light scattering, *Nano Lett. 3*, 935−8.
23. Moskovits, M. (1985) Surface-Enhanced Spectroscopy, *Rev. Mod. Phys. 57*, 783−826.
24. Junge, W., Panke, O., Cherepanov, D. A., Gumbiowski, K., Muller, M., and Engelbrecht, S. (2001) Inter-subunit rotation and elastic power transmission in F_0F_1-ATPase, *FEBS Lett. 504*, 152−60.
25. Nakanishi-Matsui, M., Kashiwagi, S., Hosokawa, H., Cipriano, D. J., Dunn, S. D., Wada, Y., and Futai, M. (2005) Stochastic high-speed rotation of *Escherichia coli* ATP synthase F1 sector: The ϵ subunit-sensitive rotation, *J. Biol. Chem.* (in press).
26. Yasuda, R., Noji, H., Yoshida, M., Kinosita, K., and Itoh, H. (2001) Resolution of distinct rotational substeps by submillisecond kinetic analysis of F-1-ATPase, *Nature 410*, 898−904.
27. Panke, O., Gumbiowski, K., Junge, W., and Engelbrecht, S. (2000) F-ATPase: Specific observation of the rotating c subunit oligomer of EFoEF1, *FEBS Lett. 472*, 34−8.
28. Cheng, L., Fenter, P., Nagy, K. L., Schlegel, M. L., and Sturchio, N. C. (2001) Molecular-scale density oscillations in water adjacent to a mica surface, *Phys. Rev. Lett. 87*, 156103.
29. Zhu, Y. X., and Granick, S. (2001) Viscosity of interfacial water, *Phys. Rev. Lett.*, 8709.
30. O'Neal, C. C., and Boyer, P. D. (1984) Assessment of the rate of bound substrate interconversion and of ATP acceleration of product release during catalysis by mitochondrial adenosine triphosphatase, *J. Biol. Chem. 259*, 5761−7.

BI052363N